This project is funded by the European Union

Final report WP6 (detectors)

Issue 1.0

Written by

Jan-Willem den Herder
Lourdes Fabrega
Flavio Gatti
Claudio Maculli
Marco Barbera
Xavier de la Broise
Jean-Luc Sauvageot
Jan van der Kuur
Mikko Kiviranta
Gao Jian-Rong

Distribution Date

22 February 2019

1 Introduction

Detailed progress reports have been provided in the past and we summarize their main results and the final conclusions in this report. As such these should be read together with the periodic progress reports and some additional WP6 related reports (AHEAD-WP6-REP-001/2016, AHEAD-WP6-REP-005/2016 and AHEAD-WP6-REP-006/2017).

There have been to face-to-face meetings by the team. For funding reasons we have not organized a dedicated close-out meeting but this was also not needed as most of the members in the team are part of the proposal for the AHEAD advanced community and as such, part of this proposal is a logical continuation of this work and part are new initiatives.

The key people in this work package are listed below including their home institutes

Institute	Key person (Name)	Role
SRON	Jan-Willem den Herder	WP 6 manager
SRON	Gao Jian-Rong	Lead X-ray detector task
SRON	Jan van der Kuur	Main contributor AC read-out task
VTT	Mikko Kiviranta	Lead Read-out task
CSIC	Lourdes Fabrega	Lead Mo/AU detector task
CEA	Xavier la Broise	Lead cryogenic harness task
Iniversity of Palermo	Marco Barbera	Lead optical filter task
INAF	Claudio Maculli	Lead anti-co optimization task
INFN	Flavio Gatti	Lead anti-co development task
Lancaster University	Alexander Kuzorezov	Lead X-ray detector modelling task

2 Report

2.1 Task 1: Management

Management activities were carried out as planned. Progress reports have been produced as planned including two face-to-face meetings (Utrecht and Barcelona) and detailed reporting in the two progress reports and various WP6 reports: AHEAD-WP6-REP-001/2016, AHEAD-WP6-REP-005/2016, AHEAD-WP6-REP-006/2017.

It was decided to organize no close-out meeting (to save resources). However, on the other side, all participants in this WP agreed to co-propose follow-on activities as part of the AHEAD proposal for an advanced community.

2.2 Task 2: Next generation of Sensors (SRON)

2.2.1 Task.2.a: Next generation of sensors (SRON)

In this WP we aim for a) define most promising improvements using TiAu bilayer as for TES (absorbers, thermal links, number of thermal links, thermal properties of substrate); b) Produce test detectors with improved performance; c) Characterize detector performance and document results. As we will describe below, we have made considerable progress with regard to the design, fabrication, and characterization:

Fabrication and devices

After demonstrating the SRON pixel with a good energy resolution of 3.9 eV X-ray resolution at 6 keV, we aim to realize a k-pixel array, and in parallel we also introduce different designs to further optimize the energy resolution for single pixels in the same wafer. To realize the k-pixel array, we need to change the wiring scheme, from a usual coplanar line scheme to a micro-stripline structure, because of the wire density and the inductance of the wires. The micro-stripline, based on a sandwich structure of a superconducting Nb layer, an insulator layer of SiO2 and a Nb layer, is the solution. We have developed a micro-stripline fabrication process, allowing a wire space of order of 2 μm, being crucial for a k-pixel array. The striplines without TES works well and show good superconductivity experimentally. So, we introduce the micro-stripline wiring into new arrays. TESs in the array have been updated to match the required geometry (a simple rectangular shaped TES, optimized wiring and TES resistance and devices). Three of such batches were fabricated. Although optical and SEM photos show good devices in the arrays, unfortunately one of the Nb layer causes a short circuit across TiAu TESs, making them impossible to be characterized further. Two new routes to fabricate arrays have been proposed, 5 batches with two different fabrication routes by two process engineers, are now in process. We expect a working k-pixel, together with many single pixel TESs, by the middle of March this year.

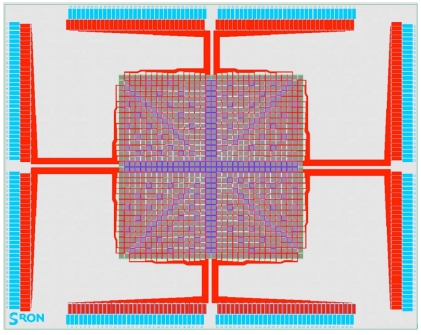

Figure 1, Designed layout of a k-pixel TES micro-calorimeter array

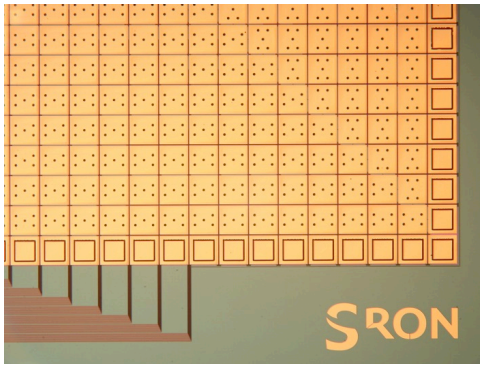

Figure 2, Optical micrograph of a fabricated

Test setups

SRON has so far only two Leiden Cryogenics coolers for measuring TES. We need a third cooler as there are increasing demands for measurement time and as two of these coolers are at an age where refurbishing becomes relevant. The latter usually takes considerable time. SRON has recently received a new mK cooler produced by Leiden Cryogenics, financially supported by ESA. The cooler shows the same performance at SRON as what measured at Leiden Cryogenics. Currently we are introducing looms/wires and also TES housing into the cooler, allowing later the measurements of an array using FDM. Also for the first time at SRON, we are going to put an X-ray source outside the cryostat. The x-ray photons will be illuminated to TES through a window on the cryostat.

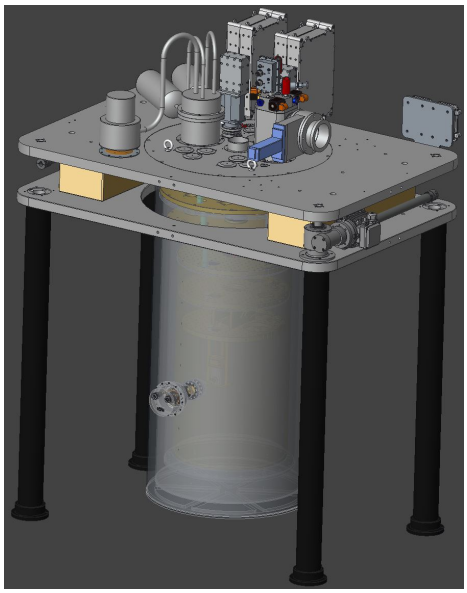

Figure 3: CAD drawing of the newly arrived Leiden coolers

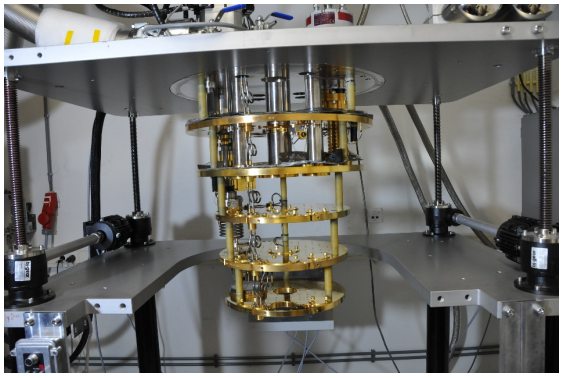

Figure 4: Open LC, the newly arrived Leiden cooler

In parallel, we have developed an acoustic mechanical attenuator, based on a two-stage mass-spring system in an existing Leiden cooler at SRON, to eliminate the cryocooler-induced low frequency noise observed in low temperature TES-based radiation detectors under development for the instruments of the next generation of infra-red and X-ray space observatories [SRON1].

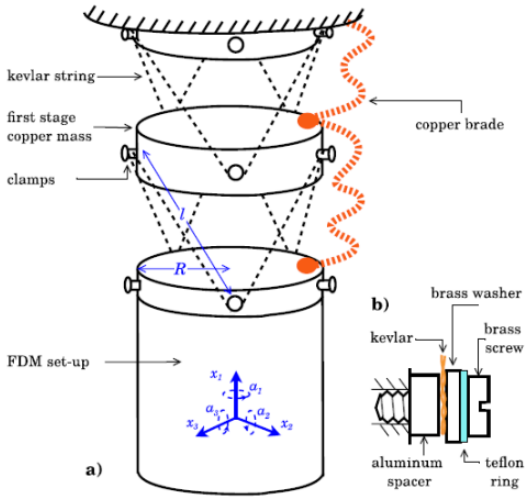

Figure 5 . (a) Schematic drawing of the two-stage mechanical attenuator developed to reduce micro-vibration induced noise in a TES bolometers array. (b), has been used to suspend each mass. The wires triangular configuration provides bending stiffness and comparable attenuation in all the six degrees of freedom.

Test results

With existing SRON TES micro-calorimeters, we have developed an important tool to characterize TES micro calorimeters, that is the complex impedance of TESs under AC bias using FDM readout system. Complex impedance measurement of a TES is the only technique that can give all the information at once, but it has been established only for a single pixel under DC bias. We have developed a complex impedance measurement method for TESs that are AC biased since we are using a MHz frequency domain multiplexing (FDM) system to readout an array. The FDM readout demands for some modifications to the complex-impedance technique and extra considerations, e.g. how to modulate a small fraction of the bias carrier frequencies in order to get a proper excitation current through the TESs and how to perform an accurate demodulation and recombination of the output signals. Also, it requires careful calibration to remove the presence of parasitic impedances in the entire readout system. We perform a complete set of AC impedance measurements for different X-ray TES microcalorimeters based on superconducting TiAu bilayers with or without normal metal Au bar structures. We discuss the statistical analysis of the residual between impedance data and fitting model to determine the proper calorimeter thermal model for our detectors. Extracted parameters are used to improve our understanding of the differences and capabilities among the detectors and additionally the quality of the array. Moreover, we use the results to compare the calculated noise spectra with the measured data. The manuscript summarizing this work by E. Taralli et al has been submitted to an AIP journal (AIP advances).

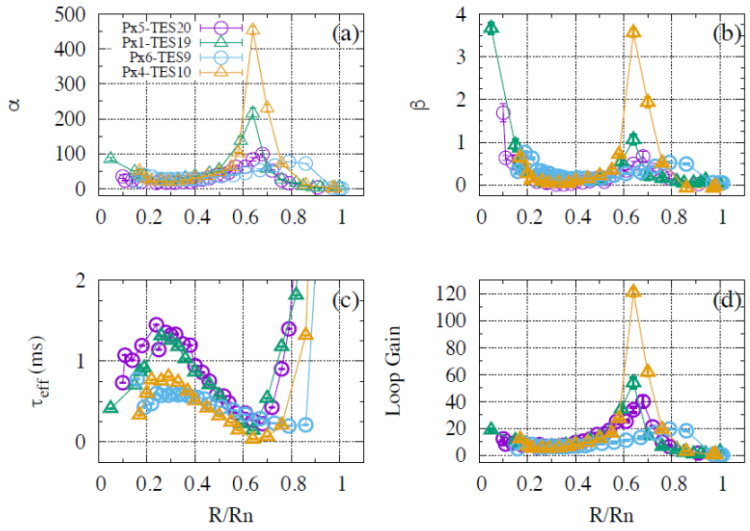

Figure. 6. Parameters of TES microcalorimeters derived from impedance measurements: α (a), β (b), τ_{eff} (c) and $\mathcal{L}$ (d) for TESs with bars over the measured bias points. Values of τ_{eff} corresponding to bias points R/R_N higher than 0.9 are intentionally maintained out of scale in plot *c*. Errors have been propagated but the corresponding error bars are too small to be properly appreciated from the plots. Lines serve no other purpose than to guide the eye.

2.2.2 Task 2.b Next generation of sensors (CSIC)

The purpose of this sub-work package was to develop the technology needed for an alternative TES using Mo/Au bilayers. The production and the properties had to be realized in order to identify if this is an alternative for the baseline Ti/Au TES.

- Mo/Au TES fabrication process was defined, with high yield and T_c reproducibility. Several wafers of TESs (T_c~100mK) with different area and designs were fabricated using Nb and Nb/Mo wiring on membranes with different thickness and area [CSIC1] (Fig.7). Electrodeposited mushroom-shaped Bi, Au and Bi/Au absorbers were included in some wafers, while other had bare TESs.

- Study of the basic properties of the constituent layers for both the absorber and the sensor was performed [CSIC2,CSIC3]. Noticeably, the evolution of T_c of Mo/Au bilayers with different Mo and Au thicknesses was tracked, in order to produce sensors with different R_n.

- The setup for full dark characterization of TES, which includes I-V, Z(ω) and noise measurements, was developed, allowing extraction of TES basic parameters (G, K, n, C, P, α, β and τ).

- Different devices were tested using full dark characterization. Results look quite promising (Fig.8) and evidence excellent transitions without banks being required [CSIC4]. Analyses of the

performances of tested devices allowed identification of routes for fine tuning of performances of Mo/Au detectors, such as increasing R_n and aspect ratio, and reducing TES area.

- A study of the transition R(T,I,H) of bare Mo/Au TESs was performed [CSIC5]. The possible role of vortex pair unbinding in the lower R region and its consequences for TES operation were analysed.

- Comparison of Ti/Au and Mo/Au devices was carried out by:
  - DC measurements of SRON Ti/Au devices in CSIC facilities. These measurements allowed comparison of DC and AC test results, and have provided the first inputs for comparison of Mo/Au and Ti/Au performances.
  - Modelling of Mo/Au devices by the University of Cambridge.

- Lastly, cryostat insert was refurbished to allow in the future spectral resolution measurements, which will help further optimization of Mo/Au devices.

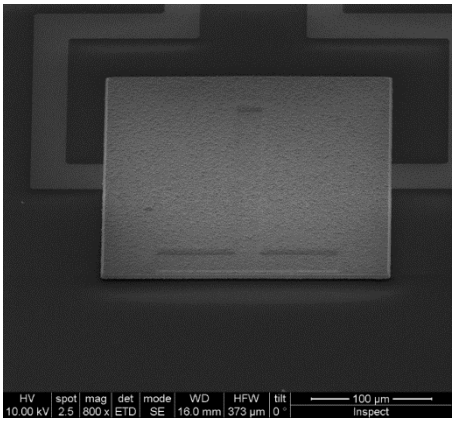

Figure 7. SEM images of a Mo/Au detector with a cantilevered electro-deposited Au absorber (240μm-wide) on its top.

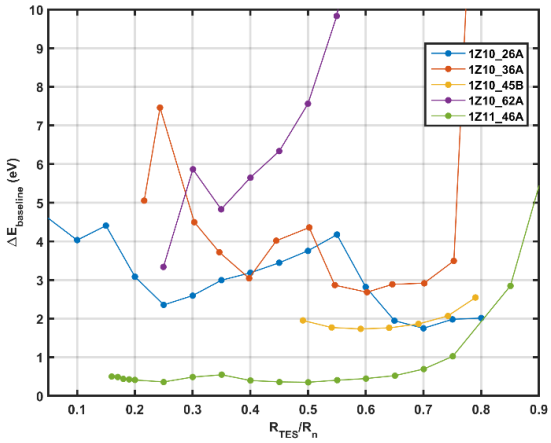

Figure 8. Baseline spectral resolution obtained from NEP at 50mK, for some tested devices. All of them have electrodeposited Au absorbers of different volumes, except 1Z11_46A, which is a bare TES with thinner Mo/Au bilayer (R_n=29 mΩ) and 50x50 μm area.

2.2.3 Task 2.c: physics modelling of sensors (Lancaster)

The purpose of this work package is to improve our understanding of the physics of a TES with absorber as X-ray detector. This is considered to be essential to optimize the detectors, most of the experimental work has been done on a TES from NASA Goddard but, for the physics, this does not matter. The main outcome of this work package was a proper model of a TES detector describing the so-called weak link effect (See L Gottardi, H Akamatsu, J van der Kuur, SJ Smith… - IEEE Transactions on Applied Superconductivity, 2017 and L Gottardi, SJ Smith, A Kozorezov, H Akamatsu… - Journal of Low Temperature Physics, 2018) and this enabled an improved design of our future devices showing that the energy resolution of a calorimeter/TES combination under AC bias can be better than 2.5 eV. In Fig. (1) we have plotted the non-linear TES impedance for the 100, 120 and 140 *u*m devices with normal metal stripes from NASA-Goddard. The three pixels are biased respectively at frequencies of 3.3, 1.7 and 2.7 MHz and our model predicts the key characteristic features observed in the measurements

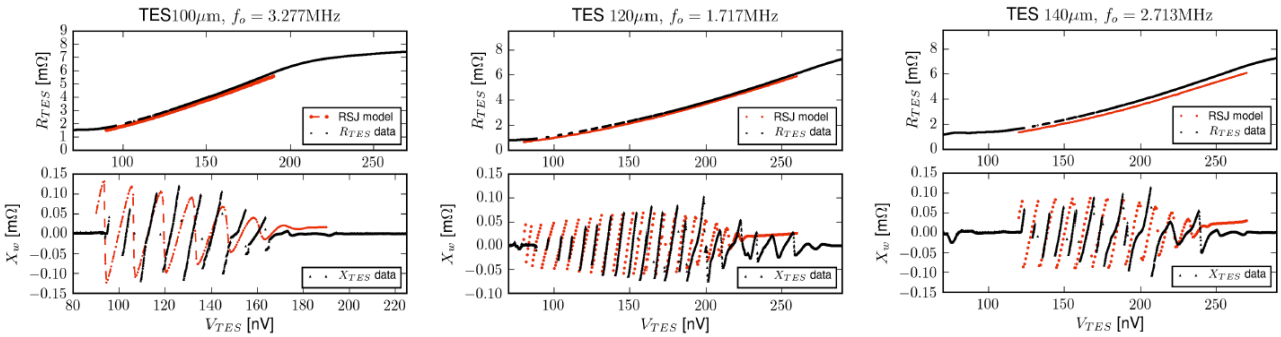

Figure 9. TES resistance and reactance of the 100, 120 and 140um pixels. The red dashed curve shows the RSJ model applied to the TES's [SRON2]

2.3 Task 3: AC biased readout (VTT)

The goal of this work package is to explore the options for further optimization of the FDM readout concept, beyond the baseline FDM system design for X-IFU.

The Task 3 co-funded with the European Space Agency (ESA) a fabrication round of Superconducting Quantum Interference Devices (SQUIDs) (Figure 10), and funded the design of a set of novel SQUID circuits for Frequency Domain Multiplexed (FDM) readout of TES detector arrays. Additionally, the Task 3 funded the early stage development towards so-called reticle-level cryogenic testing of SQUID devices.

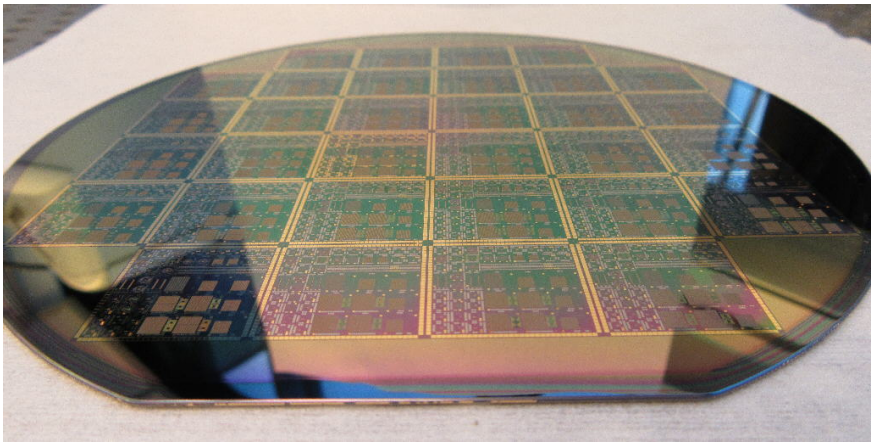

Figure 10. One of the ESA/AHEAD co-funded wafers.

2.3.1 Novel readout concepts and devices

These concepts aim to improve the TES array readout beyond the baseline design pursued by ESA.

- The first concept is a push-pull amplifier, which attempts to reduce the heat generation by SQUID amplifiers at millikelvin temperatures. The motivation is to reduce the required refrigerator capacity and thereby the launch mass of the X-IFU instrument. The amplifier concept was demonstrated with standard SQUID chips, and is described in ref. [VTT1].
- The second concept is a more efficient new way to combine the TES signals for multiplexing. A special SQUID chip designated as 'G3' was used in the demonstration, as described in ref. [VTT2].

- The third concept of 'local linearization' attempts to improve the dynamic range of the SQUID amplifier. In the X-ray calorimeter readout the TES signal swing associated with an x-ray event tends to exceed the dynamic range of the SQUID. In the conventional FDM readout, negative feedback in the form of so called Baseband Feedback (BBFB) through the room-temperature electronics is utilized. BBFB however imposes limits on intercarrier distance in frequency domain, hence limits the obtainable multiplexing factor. In the local linearization concept, neqative feedback around the SQUID within the cryogenic stage is arranged. The idea is that the BBFB only statically nulls the FDM carriers, but does not need to respond to the x-ray events. In contrast, the events will be handled solely by the extended SQUID dynamic range. In the task 3 we implemented a bias-reusing 2-stage booster amplifier, and a loc-linearized front-end SQUID for the purpose. A demonstration of the loc-linearized SQUID is shown in Figure 11.

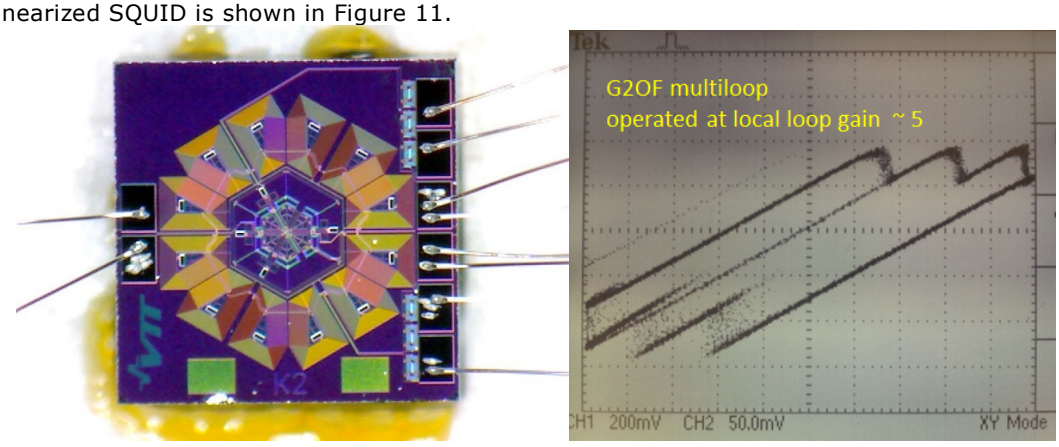

Figure 11. (Left) A locally-linearized SQUID chip implemented in Task 3. (Right) Flux response of a locally-linearized SQUID shows proper operation, except for the mediocre stability leading to flux jumps evidenced by 'ghost lines'.

2.3.2 Reticle level testing

Because testing of SQUIDs must involve cooling to the 4.2 K temperature in liquid helium, testing of individual SQUID chips is labor intensive and tedious. The so-called reticle level testing would utilize larger chunks of silicon ('reticles', Figure 12), containing order-of 20 SQUID chips, all of which could be cooled and tested as a single operation. Each chunk is small enough so that it can pass through the neck of a liquid helium storage dewar. At the perimeter of the chunk there are large-enough pads for contacting with pogo pins, so that wire bonding can be avoided. In the dicing alleys between the SQUID chips there is the integrated test wiring which leads from the perimeter pads to the SQUIDs, and which gets destroyed when the chunk is diced into individual chips after the cryogenic test. In the task 3, the said perimeter pads and test wiring were designed, and fabricated as a part of the SQUID FAB round. The reticle will get connected to test electronics via a test fixture, under development in another project and shown in Figure 13.

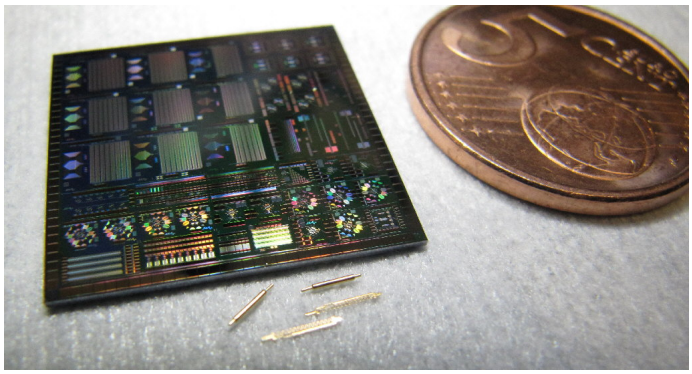

Figure 12. A 20 x 20 mm reticle containing several 4 x 4 mm and 2 x 2 mm sized SQUID chips, with test wiring in the dicing alleys and large-side test pads at the reticle perimeter. Also shown are some commericial pogo pins, intended for contacting. The reticle has been fabricated as part of the Task 3.

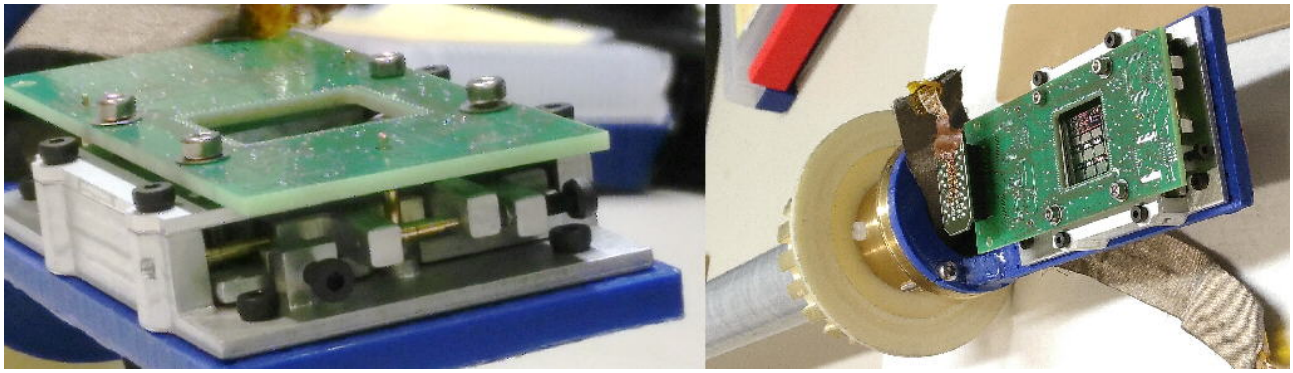

Figure 13. (Left) A miniature X-Y-θ -aligning test fixture for pogo pins, to be inserted into a storage dewar through a $\varnothing$ 50 mm neck, under development outside the AHEAD project. (Right) The test fixture attached to a liquid helium dipstick.

2.3.3 Impacts

- Although basic demonstration of the push-pull and local linearization approaches was successful, their further development to a more mature level has been delayed owing to lack of funding outside AHEAD. Currently the baseline FDM design for the X-IFU instrument has advanced sufficiently far that novel concepts are unlikely to get involved.
- The power combiner approach is likely to be applied in the next-generation design of the LC resonators for the X-IFU instrument.
- Final demonstration of the reticle level testing is still pending, but if successful, will be applied in regular SQUID production. Reticle level testing will significantly lighten the test efforts once the X-IFU flight hardware will need to be delivered.

2.4 Task 4: Anti-coincidence detectors (INAF)

This task 4 is aimed at improving the ATHENA X-IFU Cryogenic AntiCoincidence (CryoAC) detector beyond the present baseline, in order to provide both a scientific capability and an improvement of the particle rejection efficiency. We remind that the CryoAC (4-pixels array having about 1.2 cm^2 area each pixel, 500 um silicon thick) is a TES-based detector aimed at reducing the particle background around the main TES-array instrument: the lower the particle background, the higher the X-IFU instrument sensitivity.

A) CryoAC spectroscopic capability

The aim of this task has been to provide a feasibility study to improve the baselined anticoincidence detector towards some spectroscopic capability. From the scientific point of view it is interesting because could extend the X-IFU working bandwidth up to 20 keV where the main detector has a reduced quantum efficiency.

By considering the CryoAC Silicon absorber thickness (500 um), the effective area of the ATHENA optics (~ 1 cm^2@20keV), the presence of both the thermal filters and the TES-array above the CryoAC it has been shown that an extension up to 20 keV is feasible by requiring to the CryoAC an energy resolution of ~ 2 keV@20keV [INAF1]. It is worth of note that the thickness of the CryoAC ensures good quantum efficiency at this energy range (~ 40%). It has been demonstrated that this response is relevant to several tens of HMXB (High Mass X-ray Binaries) objects. With the increased bandwidth of the CryoAC the significance of the critical astrophysical parameters (Ec and EF are the cut-off and fold energies), will be constrained for these sources. From the technological point of view, as result from three different concept studies, the more solid viable solutions foresee a careful selection of Si absorbers as task to be carried out to reach the goal. During the 2nd reporting period, we have performed some test activity on Si samples (see Fig. 14), related to the chip developed for the baseline detector that has been backside illuminated by photons (Fe55) showing good energy resolution ~ 3keV@6keV. This has provided the intrinsic feasibility to obtain some spectroscopic information from these devices [INAF2] as requested by the analysis reported in [INAF3].

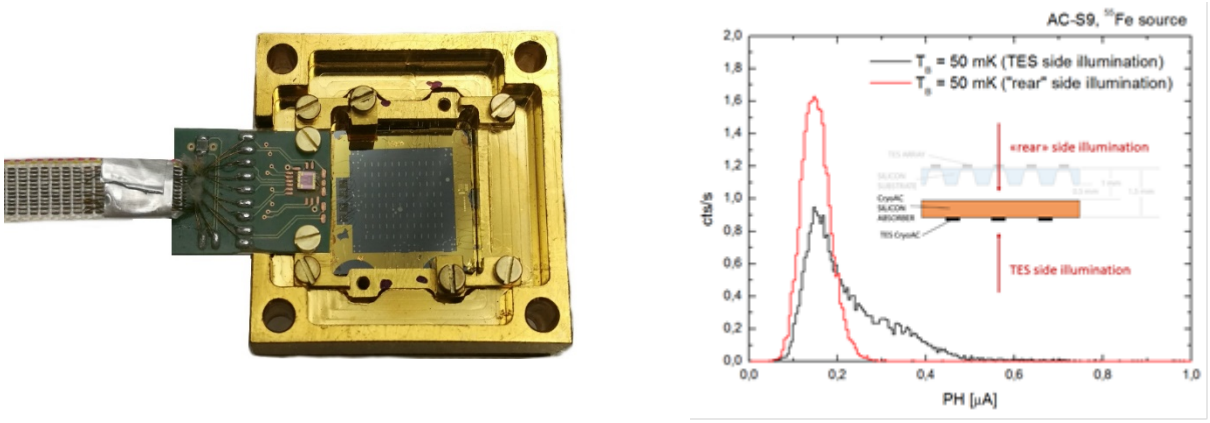

Figure 14. Left- AC-S9 chip inserted in the sample holder. Right – 6 keV energy spectrum by illuminating the sample on front and backside.

At present, in the context of the DM CryoAC activity for ATHENA, a new sample made of a suspended Si absorber is under test, whose preliminary results are quite promising in term of spectroscopic capability (<

2keV@6keV) showing the relevance of the work carried out under AHEAD for the research infrastructure Athena.

B) Improving of the particle rejection efficiency

This task is linked to WP7 activity since it involves particle background evaluation. The focus has been to assess an alternative design wrt the CryoAC baseline, in order to increase the rejection efficiency. Being secondary particles emitted by the main detector neighbourhood the main component of the residual particle background, what we can do is to limit its production or put a veto, the latter implying a detection of such particles.
To do so, two tasks have been accomplished:

1. Inserting a Kapton/Bi liner inside the FPA superconductive Nb shield to reduce the production of secondaries
2. Adding a lateral detectors, at 90 degree wrt baselined planar CryoAC has been added, thus improving the detector solid angle coverage

The main work in the context of WP6 has been design of such solutions performed in collaboration with the SRON team leading the development of the X-IFU FPA.

Both the tasks have been reported in the previous reporting period. The first solution permitted to reach the requirement on the residual particle background (5E-3 cts/cm^2/s/keV), the second one to reduce this value by a factor ~ 2. They have been both proposed to the Athena X-IFU team and the first one has been adopted in the present baseline configuration, while the second one has not been accepted because of a huge reworking of the present baseline FPA.

2.5 Task 5: Interconnecting harness for cryogenic detectors (CEA)

The purpose of this task is to improve the interconnecting harness between 50 mK and 2/4 K to enable a large number of signal wires while keeping the thermal load and cross talk low. The harness we have designed contains 37 tracks, routed on a signal layer, which is interleaved between two shielding layers made of hatched shielding planes, and this set is again interleaved between two thermal contact layers where large gold pads are designed at both extremities of the harness and at its middle, for thermalization at three different temperatures. All the grounds of the four top layers are interconnected by microvias, in order to entirely enclose the lines by shielding, and to improve the thermalization. The width of the signal tracks is 15 µm spaced by 15 µm, the length of the harnesses is 100 mm, its maximal width (at connector level) is 19 mm, and its minimal width (between two thermal contacts) is 1.89 mm.

CEA ended the design of the harness in August 2016, and Hightec, the manufacturer, delivered a first batch in February 2017. Then CEA has performed a systematic detailed visual inspection of the prototypes : the overall result was good, but many local defects were observed (only three panels over the six produced were partially OK). In parallel, CEA performed cold tests ; in particular, the critical temperature of the tracks has been measured, and the obtained value (9.2 K) was very close to that of the bulk niobium (9.3 K) : this excellent result is due to a good deposition quality.

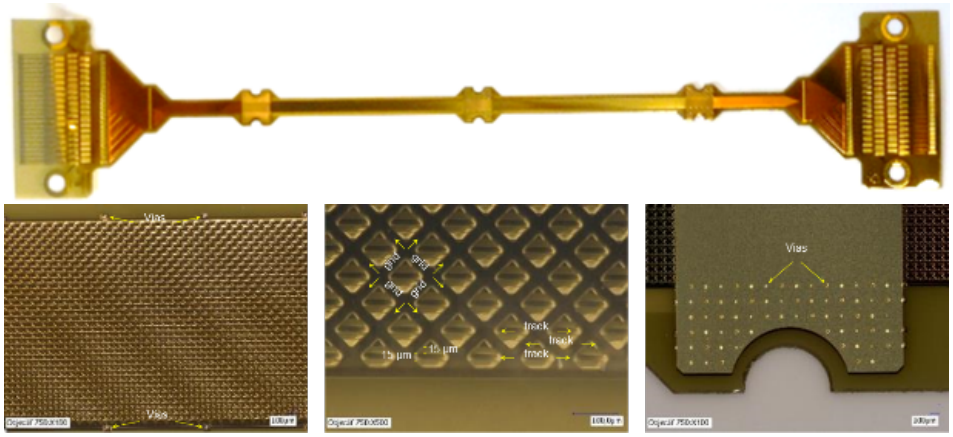

Figure 15. At top : photograph of the harness. At bottom, left : zoom on the tracks and grids zone ; the shielding grids are closed by vias. Middle : further zoom where 15 µm/15µm tracks appear between the two shielding grids. Right : zoom on a top thermal contact, with vias connecting it to the two shielding planes.

Two months later (April 2017), the manufacturer delivered a second batch, complementary to the first one, where the yield was better and several defects were fixed : this was mainly the result of an improvement of the adjustment of the process parameters. But unfortunately the adhesion defects, observed on the previous batch, fully persisted. Whereas the other remaining defects were not critical and were more appearance defects, the problem of the delamination was critical, because it prevents to use properly the affected harnesses. This defect appeared on the connector large pads, completely or partially delaminated, and also on the thermal contact pads.

This is the reason why we decided to stop the production and to produce a special batch containing test samples and simplified harnesses (containing only the signal layer), in order to test and compare several modified processes, including new adhesion layers and activation methods. This special batch has been delivered in June 2017, and pullout tests were performed by the manufacturer and cold tests by CEA, in order to compare the solutions. Finally, a new adhesion layer has been validated to solve the problem.

This new adhesion layer has been integrated in the process, and a third batch has been launched (this is an extra production, originally not foreseen in the AHEAD plan). This batch has suffered of several restarts from zero (process duration : three months), due to several machine problems during the production while the batch manufacturing was very advanced, so that its delivery occurred in December 2018.

CEA did a detailed microscopic inspection of these new samples, and analysed the results of the systematic measurement at ambient temperature of the resistance of all the tracks, which is a precise indicator of the deposit quality of metallisation. The results are very good : the delamination problem disappeared, the yield is very high with very few open tracks, and the resistance values are homogeneous and nominal. We are currently conducting the low temperature measurements. We have already controlled the critical temperature of tracks : again, the obtained value is excellent (9.25 K), and there is no dispersion from a track to another. Moreover, the critical current is very high. The next step will be the measurement of the thermal conduction of this new batch ; it will be done very soon.

Another important task to perform was the equipment of the harness. Connectors or wire bonding should be implemented at both extremities, for electrical interconnection of the harness. This require firstly gluing

stiffeners at both extremities (these stiffeners are also used to thermalize the harness). To this aim, CEA has developed a specific heating controlled press (see figure below). For the implementation of the connectors, our will was to use an « almost » classical PCB solder brazing process (solder paste through stencil) but using a low temperature solder paste (96°C) adapted to our glue. For setting the soldering process, we have developed many supports and tools (for example a jointed tray for positioning the harness in the brazing machine : see figures below) and made several trials. We have arrived at a satisfactory result and are now proceeding to the last adjustments.

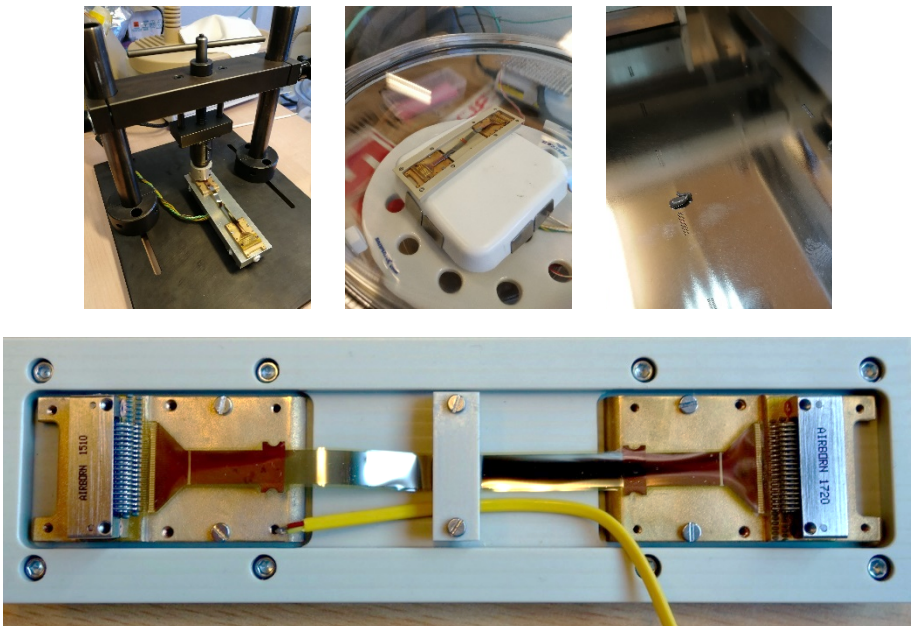

Figure 16. At top, from left to right : photo of the harness under the heating controlled press for the gluing of the stiffeners ; harness in the oven for baking before brazing of connectors ; stencil upon the harness for spreading of the solder. At bottom : A harness in its jointed tray, fully equipped with nanoD connectors, at the exit of the brazing oven ; the yellow cable connects the thermocouple used to precisely control the temperature during the brazing.

To conclude, the progress of the manufacturing of the superconducting flexible PCB has been delayed by the occurring of critical defects of adhesion (delamination) for the large pads (connector and thermal contact pads). But a good cooperation has been performed with the manufacturer to identify and solve the problem. A modified process has been validated, and the last produced prototypes are fully satisfactory. The manufacturer has progressively improved its mastery of the process, and it seems today to be able to produce good quality harnesses in reasonable time. So, the technology seems to be now mature for a use in a spatial experiment. Moreover, we have developed the processes and the tools to equip the harnesses with nanoD connectors and to characterize and qualify them at cold.

2.6 Task 6: Optical blocking filters for cryogenic detectors (University of Palermo)

The purpose of this work package was to design, develop and characterize optical blocking filters for cryogenic X-ray detectors operating in Space with the main goal to get high transmission in the soft X-rays still providing the required attenuation of radiative thermal load from warm surfaces in the instrument, of optical/visible light from astrophysical sources, and of radio frequency EMI from the spacecraft operation. The filters have also to protect the detector from molecular contamination and, despite being very thin, they shall withstand severe launch mechanical stresses.

A significant and driving case study in this WP was the development of the X-Ray Integral Field Unit (X-IFU), a TES microcalorimeter array detector on board the European Space Agency large mission ATHENA. Indeed, one of the major outcome of this task activity is the definition of the conceptual design of the ATHENA X-IFU thermal filters (TF) stack consisting of five identical filters each one with a thin polyimide membrane (45 nm thick) coated with aluminum (~30 nm thick). The TF operates at different temperatures namely: 300 K, 100 K, 30 K, 2 K, and 0.05 K, corresponding to the temperatures of the shields of the cryostat. The three outer and warmer filters will be mounted on the Aperture Cylinder (AC) of the cryostat while the two inner and coldest filters will be directly mounted onto the Focal Plane Assembly (FPA) (Figure 17).

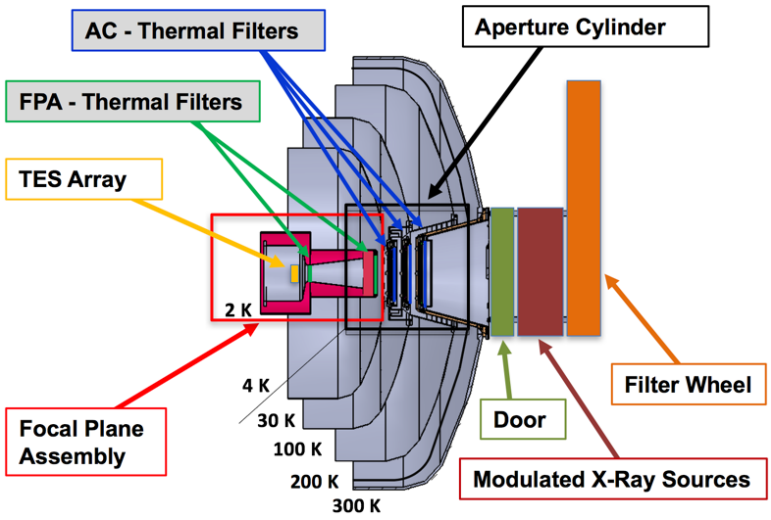

Figure 17. Thermal filters configuration in the general layout of the X-IFU Focal Plane Assembly and Detector Cooling System. Highlighted in light grey are the thermal filters.

To increase the mechanical robustness, the thin Al coated polyimide films will be supported by a honeycomb mesh made of SS 304 plated with 5 μm of Au for the outer filters, and of Nb for the coldest filter operating at 50 mK inside the FPA. The meshes, which are designed to have < 3% geometric blocking factor with typical cell sizes ranging between 2 and 5 mm, provide also thermal conductance and contribute to attenuate the RF radiation below 6 GHz.

Figure 18 shows a comparison between the X-ray transmission of the investigated stack of thermal filters for the Athena X-IFU (red) and that of the thermal filters mounted on the X-ray microcalorimeter spectrometer on-board ASTRO-H (blue). While the significant gain obtained at soft energies is very encouraging, the use of metal meshes implies a transmission at high energy lower than ASTRO-H. The investigated X-IFU TF stack

design is consistent with the requirements (horizontal black marks), namely: 21% @ 0.35 keV, 76% @ 1 keV, and 89% @ 7 keV.

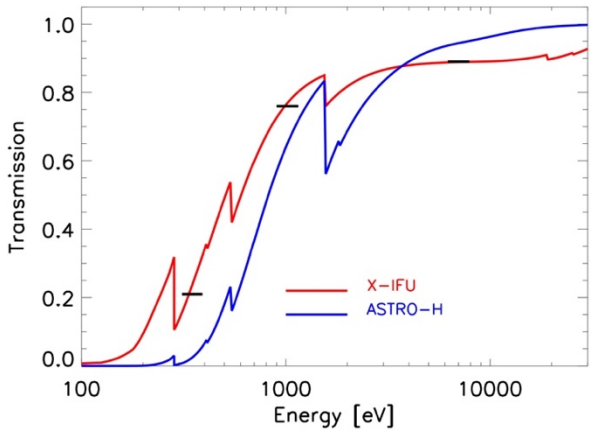

Figure 18. X-ray transmission of the stack of thermal filters investigated for the Athena X-IFU (red line) compared to the response of the thermal filters mounted on the X-ray microcalorimeter spectrometer on board ASTRO-H (blue line). The requirements are showed with horizontal black marks.

A few filter samples have been procured along this project to characterize optical and mechanical properties of the investigated materials and support the design optimization, namely:

- **Large size filters** (I.D. = 56-100 mm) consisting of Ti coated polypropylene (~ 700 nm thick) supported by SS 304 meshes built to test meshes under static and dynamic loads.
- **Medium size filters** (I.D. = 30 mm) consisting of Al coated polyimide (45 nm thick) supported by Au plated SS 304 meshes built to test the thin foils under static and dynamic load, to perform thermo-vacuum tests, and X-ray absorption spectroscopy and imaging (Figure 19).
- **Small size filters** (I.D. = 15 mm) consisting of Al coated polyimide meshless to perform optical measurements, surface investigation, and X-ray absorption spectroscopy.

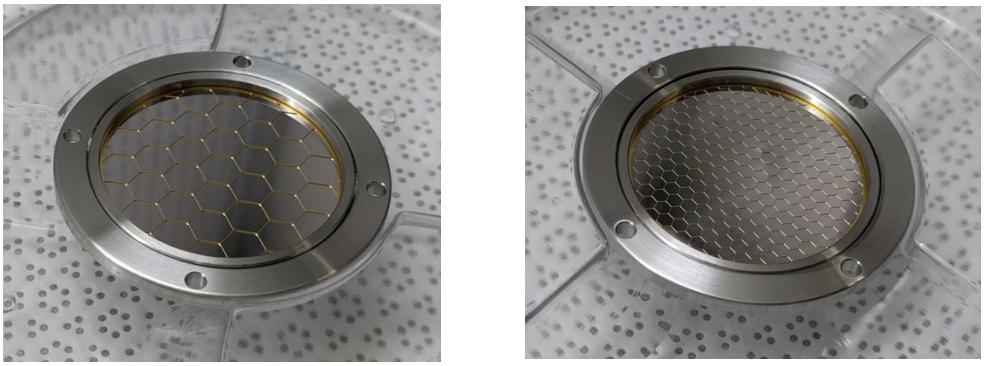

Figure 19. Polyimide film (45 nm thick) coated with aluminum (30 nm thick) supported by Au plated SS 304 meshes mounted on standard TF130 LUXEL frames with 30 mm clear aperture diameter. The filter on the left has a mesh with 5 mm pitch and wires 65 µm X 130 µm (w X h), while the one on the right has a mesh with 2 mm pitch and wires 30 µm X 60 µm (w X h).

Sine and random vibration tests have been performed on large and medium size filters at the Centre Spatial de Liege (Belgium) and Max-Planck-Institut fuer extraterrestrische Physik (Garching, Germany). All tested filters have survived vibration levels larger than the Ariane 5 reference specifications [Barbera, M. et al. 2018, Parodi, G. et al. 2018].

A set of large size and medium size filter samples, mounted inside a vacuum tight box (Figure 20, right panel), have also been exposed to the Ariane 5 acoustic reference load at AGH University of Science and Technology in Krakow (Figure 20, left panel). Different tests have been performed with filters kept at pressure < 1 mbar, 10 mbar, 100 mbar and 1000 mbar pressure and all filters have survived the acoustic load in all mentioned conditions. This preliminary test suggests that the option of launching the cryostat in residual pressure (currently not the baseline) can be taken into account although it needs further investigation [Barbera et al. 2018].

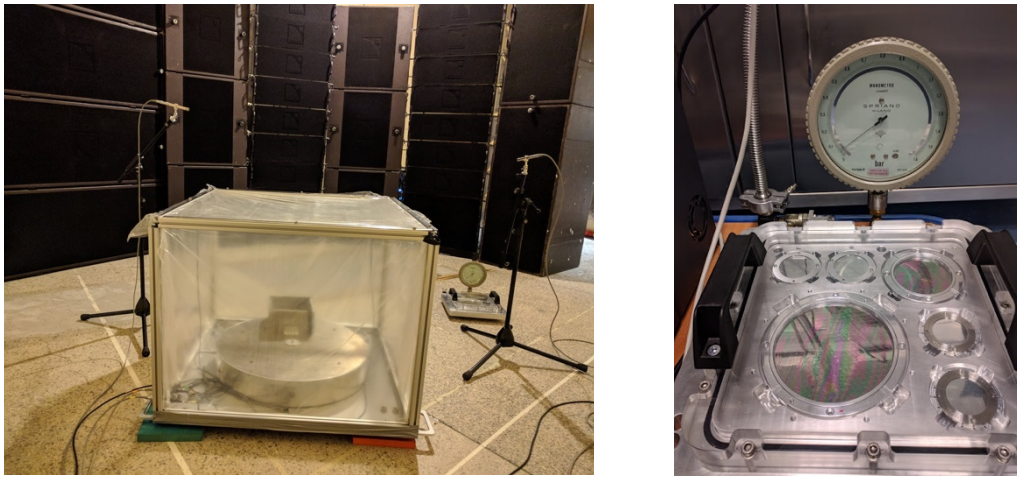

Figure 20. Test equipment inside the AGH reverberation chamber (left panel). The plastic tent in foreground covers the filter wheel mock-up used to test filter samples of the ATHENA Wide Field Imager, while the vacuum tight box used for the X-IFU filters acoustic tests is in the background. The right panel shows the tested X-IFU filter samples mounted inside the vacuum tight box.

Preliminary thermo-vacuum and static differential pressure tests were also performed at dedicated facilities in UNIPA/INAF-OAPA (Palermo) on two medium size filter test samples to complement the design characterization [Barbera et al. 2018].

Radio frequency shielding efficiency (SE) has been measured on a set of aluminum thin-films with thickness in the range 10-40 nm supported by plastic foils, on hexagonal copper meshes, and on the combinations of Al films and meshes. We found that a layer of aluminum with thickness > 30 nm provides more than 30 dB attenuation at frequencies > 6 GHz (Figure 21 left panel) while at lower frequencies a metal mesh is needed to provide the required attenuation (Figure 21 right panel) [Lo Cicero et al. 2018]. Recent measurements have been performed on a stack of two metal meshes mounted in a representative configuration and have shown that the X-IFU SE requirement on thermal filters can be met in the full frequency range 60 MHz – 20 GHz.

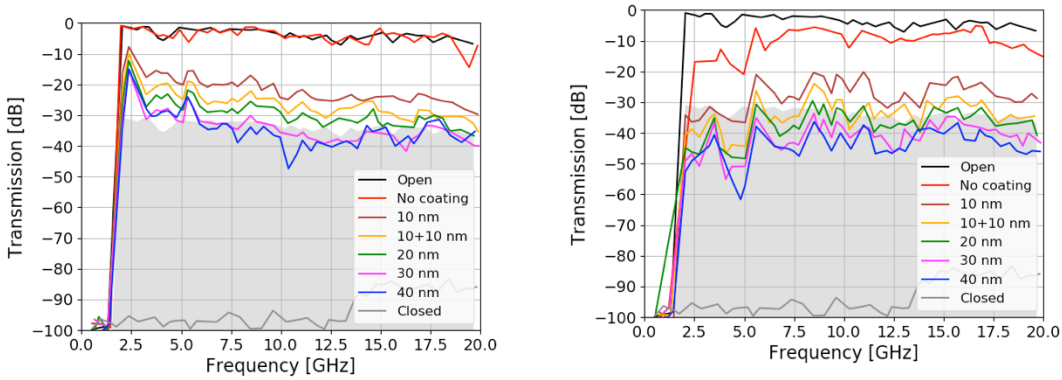

Figure 21. Measured SE of an Al film with thickness in the range 10-40 nm (left panel). "Open" and "Closed" curves show measurements without filters and with a thick Al disk, as references. "No coating" refers to the plastic substrate alone. The gray area displays where a 30 dB attenuation requirement is met. The right panel is the SE of a copper mesh combined with the Al films. In red the SE of the mesh alone.

As a result of this research activity, some options will be investigated in the near future to further improve the X-ray transmission of the thermal filters stack and thus obtain at essentially no additional cost and mass a recovery of the X-IFU effective area lost by the Athena telescope geometric area reduction imposed by cost and mass constraints. In particular, we will consider: 1) removing one of the five filters, 2) reducing the thickness of aluminium on a few filters, 3) replacing the metal mesh with a polyimide mesh on a few filters.

3 Additional results

The deliverables, milestones and publications are recorded in the EU portal. In practice the number of publications in the first phase was slow but has increased significantly. We also expect results of the AHEAD activities to be part of future publications. The team agreed to properly refer to the AHEAD contributions.

4 Conclusions and lessons learned

In conclusion we can state the following:

1) The participating institutes have developed an attitude to work together during the different phases. This will be mostly realized in the context of concrete projects but, for example, developing and testing of cryo-harness is done in a collaborative way. This is a clear success of the AHEAD activity.

2) Improved understanding of the physics realized in WP 6.2 enabled better optimization of the pixel design for Athena as there is now a proper theoretical understanding of 'weak link' effects and the AC biasing of the devices (this work had already been reported before).

3) Measurements of in-house developed sensor arrays has been slower than anticipated due to unexpected leaks in the cooling system and shorts in the produced devices. Whereas these items are solved and the work will continue, in the AHEAD program we were able to define optimized sensors designs taking into account measurements (IV curves) and the improved understanding of the physics. Unfortunately the solution to these problems takes time (one need multiple cool down cycles to understand and correct a superfluid leak in a cryostat) that final results of these improvements in terms of the energy resolution has not been demonstrated (but all intermediate steps and measurements indicate a significant improvement).

4) The work on the cryoAC was also completed in the earlier phase showing the enhanced capability of this detector to realize spectroscopic performance (including the science case) as well as illustrating options to reduce the background in the Athena mission which is now under construction. One solution, the application of graded Z-shielding in the cryogenic detector is now the baseline whereas the other improvement (increasing the solid angle covered by the cryoAC by a factor 2) is technically so complicated that it is not part of the baseline.

5) The technology for the cryo-harness has been improved thanks to AHEAD and is, in principle, ready to be used for Athena. Whereas the technology is present, further detailed design is required but this is clearly outside the scope of AHEAD. AHEAD has demonstrated the technical feasibility.

6) Improved modelling of our thermal windows/filters and corresponding measurement have revealed the capability and performance of these filters as GHz filters and also the change of the EXAFs as function of temperature have been very clearly defined. This has a major impact on the design (GHz filtering) and calibration programs of Athena.

The lessons learned are the following:

1) Enabling teams to collaborate has a much broader impact that the direct results from the work. We have clearly observed the interst to continue some of this work in European teams..

2) Development of key space technology is a long term investment. Whereas clear improvements in the capability of the Athena mission has been achieved, the full exploitation of the EU investments in this infrastructure and in particular the detector work package will require continued attention.

3) In the accomplished AHEAD activities we have explored the optimization of the Athena facility beyond its baseline and as illustrated, this resulted in various improvements which could be fitted in the current Athena baseline. It also became clear that the Athena infrastructure is not only determined by the performance of the hardware but that calibrations and modelling of the background is equally important. Topics which need more attention.

4) The investments in Athena detector technology have been started more than 15 years ago. This is not an unrealistic time horizon for cutting edge technology. EU funding can serve to enable the collaboration between current institutes and new institutes to realize improved detectors for future missions. It is now the right time frame to initiate these.

Appendix

Additional references are given below but the full set is included in earlier reports.

[SRON1] "A six-degree-of-freedom micro-vibrations acoustic isolator for low-temperature radiation detectors based on superconducting transition-edge sensors" by L. Gottardi et al has been accepted for a publication in Review of Scientific Instrument.

[SRON2] L Gottardi, H Akamatsu, J van der Kuur, SJ Smith… - IEEE Transactions on Applied Superconductivity, 2017

[VTT1] M. Kiviranta, "Low-dissipating push-pull SQUID amplifier for TES detector readout", ArXiV 1810.04706 .

[VTT2] M. Kiviranta, L. Grönberg and J. van der Kuur, "Two SQUID amplifiers intended to alleviate the summing node inductance problem in multiplexed arrays of Transition Edge Sensors", ArXiV 1810.09122 .

[INAF1] M. D'Andrea et al., "The Cryogenic AntiCoincidence detector for ATHENA X-IFU: a scientific assessment of the observational capabilities in the hard X-ray band", Exp. Astron. 44, 359 (2017). DOI 10.1007/s10686-017-9543-4

[INAF2] M. D'andrea et al., "The Cryogenic Anticoincidence Detector for ATHENA X-IFU: Preliminary test of AC-S9 towards the Demonstration Model", Proc. of SPIE Vol. 10699 106994T-1 (2018).

[INAF][M. D'Andrea et al., "The Cryogenic AntiCoincidence detector for ATHENA X-IFU: a scientific assessment of the observational capabilities in the hard X-ray band", Exp. Astron. 44, 359 (2017). DOI 10.1007/s10686-017-9543-4".

[CSIC1] P.Strichovanec, A.Camón, J.Moral-Vico, J.Sesé, N.Casañ-Pastor, C.Pobes, R.M. Jáudenes and L. Fàbrega, "Progress on the fabrication of Mo/Au Transition Edge Sensors for X-ray detection", presented at ASC2018

[CSIC2] J.Moral-Vico, N.Casañ-Pastor, A.Camón, C.Pobes, R.M.Jáudenes, P.Strichovanec and L.Fàbrega, "Microstructure and electrical transport in electrodeposited Bi films", J. Electroanalytical Acta 832, 40 (2019).

[CSIC3] L.Fàbrega, A.Camón, P.Strichovanec and C.Pobes, "Exploring the proximity effect in Mo/Au bilayers", IEEE Trans. Appl. Supercond. (proceed. ASC2018), final stages of revision.

[CSIC4] C.Pobes, L. Fàbrega, A.Camón, N.Casañ-Pastor, P.Strichovanec, J.Sesé, J.Moral-Vico, R.Jáudenes, "Development of cryogenic X-ray detectors based on Mo/Au Transition Edge Sensors", IEEE Transactions on Appl. Supercond. 27, 2101505 (2017); C.Pobes, L.Fàbrega, A.Camón, P.Strichovanec, J.Moral-Vico, N.Casañ-pastor, R.M.Jáudenes, J.Sesé, "Comparison of different Mo/Au TES designs for radiation detectors", J. Low Temp. Phys. 193, 282 (2018); C. Pobes, L.Fàbrega, A. Camón, P.Strichovanec, J. Moral-Vico, N. Casan-Pastor, J. Sesé, R.M. Jáudenes "Study of basic parameters of Mo/Au-based TES", presented at ASC2018.

[CSIC5] L.Fàbrega, A.Camón, C.Pobes, P.Strichovanec and R.González-Arrabal, "Large current-induced broadening of the superconducting transition in Mo/Au TES", Supercond. Sci. and Technol. 32, 015006 (2019)

[UniPa1] Barbera, M. et al., "ATHENA X-IFU thermal filters development status toward the end of the instrument phase-A", Proc. SPIE, 10699, 106991R (2018). Doi: 10.1117/12.2314450

[UniPa2] Parodi, G. et al., "Structural modelling and mechanical tests supporting the design of the ATHENA X-IFU thermal filters and WFI optical blocking filter", Proc. SPIE, 10699, 106994C (2018). Doi: 10.1117/12.2314451

[UniPa3] Lo Cicero, U. et al., "Radio frequency shielding of thin aluminized plastic filters investigated for the ATHENA X-IFU detector", Proc. SPIE, 10699, 106